Dry cyclogenesis and dust lofting in the intertropical discontinuity region of the West African Monsoon : A case study

Diana Bou Karam, Cyrille Flamant, Pierre Tulet, Martin C. Todd, Jacques Pelon, Earle Williams

Dry cyclogenesis and dust mobilization in the intertropical discontinuity of the West African Monsoon: A case study

Diana Bou Karam,[1] Cyrille Flamant,[1] Pierre Tulet,[2] Martin C. Todd,[3] Jacques Pelon,[1] and Earle Williams[4]

Received 8 August 2008; revised 11 November 2008; accepted 21 January 2009; published 14 March 2009.

[1] Three-dimensional mesoscale numerical simulations were performed over Niger in order to investigate dry cyclogenesis in the West African intertropical discontinuity (ITD) during the summer, when it is located over the Sahel. The implications of dry cyclogenesis on dust emission and transport over West Africa are also addressed using the model results, together with spaceborne observations from the Spinning Enhanced Visible and Infra-Red Imager (SEVIRI) and the Cloud-Aerosol Lidar with Orthogonal Polarization (CALIOP). The study focuses on the case of 7–8 July 2006, during the African Monsoon Multidisciplinary Analysis (AMMA) Special Observing Period 2a1. Model results show the formation of three dry cyclones in the ITD during a 24-h period. Simulations are used to investigate the formation and the development of one of these cyclones over Niger in the lee of the Hoggar-Aïr Mountains. They show the development of the vortex to be associated with (1) strong horizontal shear and low-level convergence existing along the monsoon shearline and (2) enhanced northeasterly winds associated with orographic blocking of air masses from the Mediterranean Sea. The dry cyclone was apparent between 0700 and 1300 UTC in the simulation, and it was approximately 400 km wide and 1500 m deep. Potential vorticity in the center of vortex reached nearly 6 PVU at the end of the cyclogenesis period (1000 UTC). The role of the orography on cyclogenesis along the ITD was evaluated through model simulations without orography. The comparison of the characteristics of the vortex in the simulations with and without orography suggests that the orography plays a secondary but still important role in the formation of the cyclone. Orography and related flow splitting tend to create low-level jets in the lee of the Hoggar and Aïr mountains which, in turn, create conditions favorable for the onset of a better defined and more intense vortex in the ITD region. Moreover, orography blocking appears to favor the occurrence of a longer-lived cyclone. Furthermore, model results suggested that strong surface winds ($\sim$11 m s^{-1}) enhanced by the intensification of the vortex led to the emission of dust mass fluxes as large as 3 μg m^{-2} s^{-1}. The mobilized dust was mixed upward to a height of 4–5 km to be made available for long-range transport. This study suggests that the occurrence of dry vortices in the ITD region may contribute significantly to the total dust activity over West Africa during summer. The distribution of dust over the Sahara-Sahel may be affected over areas and at time scales much larger than those associated with the cyclone itself.

Citation: Bou Karam, D., C. Flamant, P. Tulet, M. C. Todd, J. Pelon, and E. Williams (2009), Dry cyclogenesis and dust mobilization in the intertropical discontinuity of the West African Monsoon: A case study, *J. Geophys. Res.*, *114*, D05115, doi:10.1029/2008JD010952.

1. Introduction

[2] In recent years, increased attention has been given to the dynamic processes that control dust mobilization and transport from the arid and semiarid regions of West Africa. This dust is subsequently transported over scales ranging from local to global. The intertropical discontinuity (ITD), which marks the surface position of the interface between the cool, moist southwesterly monsoon flow and the hot, dry northeasterly harmattan flow and is also referred to as the monsoon shearline in the literature [e.g., *Sadler*, 1975], has been reported to be a key feature associated with dust emissions over West Africa. *Engelstaedter and Washington* [2007] have shown that the mean dust activity over the dust "hot spots" of the West African Sahara (about 18°N–20°N)

[1] LATMOS, IPSL, Université Pierre et Marie Curie, CNRS, Paris, France.
[2] GAME, CNRM, Météo-France, Toulouse, France.
[3] Department of Geography, University College London, London, UK.
[4] Lincoln Laboratory, Massachusetts Institute of Technology, Cambridge, Massachusetts, USA.

0148-0227/09/2008JD010952

exhibits a maximum around the monsoon onset period (June and July) in coincidence with the annual northward displacement of the ITD over the dust hot spots of the Sahel. The authors infer that emission is likely to be linked to small-scale high-wind events associated with dry convection, although direct evidence of this has yet to be confirmed. More recently, *Bou Karam et al.* [2008] have identified a new mechanism for dust emission over the Sahel in which highly turbulent winds at the leading edge of the monsoon nocturnal flow generate dust uplifting. Furthermore, studies of monsoon systems and cyclogenesis in other parts of the world indicate that the ITD, being characterized by a strong convergence and strong horizontal shear in the low levels, is expected to provide favorable dynamical conditions for cyclogenesis [e.g., *Briegel and Frank*, 1997; *Toyoda et al.*, 1999]. Over semiarid and arid West Africa such cyclogenesis may lead to strong winds and dust mobilization.

[3] *Krishnamurti et al.* [1981] have studied the vortex onset over the Arabian Sea associated with the Indian Monsoon. The development of large numbers of mesoscale vortices over the western North Pacific region has been observed during the Tropical Cyclone Motion-90 field campaign [Lander and Holland 1993]. In West Africa, the existence of mesovortices associated with the West African Monsoon has been evoked through tropical cyclogenesis studies [e.g., *Karyampudi and Pierce*, 2002] where it has been shown that the merger of low-level vortices associated with the monsoon shearline over the eastern Atlantic was at the origin of the initiation of the Tropical Storm Ernesto (1994) and Hurricane Luis (1995).

[4] *Karyampudi et al.* [1995] pointed out the role of cyclogenesis in the leeside of the Rocky Mountains on blowing dust over the Great Plains. *Qian et al.* [2002] investigated the relationship between dust storms and cyclone activity over China by conducting climatological analyses on 50-year weather data and showed that a high positive correlation was found between the annual dust weather frequency and the annual cyclone frequency. Dust mobilization by the Mongolian cyclone over China has been simulated by *Liu et al.* [2003], who demonstrated that this feature forms the major dynamic forcing pattern that mobilizes dust and that mechanical and convective turbulence play the major role in mixing the dust upward.

[5] In spite of the fact that cyclogenesis has been reported to be associated with the convergence zone of monsoon systems in several regions of the globe (mostly over the ocean), and that cyclogenesis is known to be an important dynamical process for dust mobilization and transport, no attention has been given to dry cyclogenesis associated with the West African monsoon shearline over the West African continent (recognized as the world's largest source of mineral dust [*Prospero et al.*, 2002]), and its impact on dust uplift over Sahara and Sahel.

[6] This study focuses on a dry cyclogenesis event over western Niger in the lee of the Hoggar and Aïr mountains on 7 July 2006. The event occurred during a Special Observing Period (SOP) of the African Monsoon Multidisciplinary Analysis (AMMA) [*Redelsperger et al.*, 2006]. The objectives of the study are twofold: (1) to examine the process of dry cyclogenesis in the ITD region and (2) to evaluate the role of a dry cyclone on dust emission and transport over the Sahel through three-dimensional mesoscale simulations using the mesoscale atmospheric model MesoNH and spaceborne observations.

[7] The paper complements those of *Bou Karam et al.* [2008; also Estimate of Sahelian dust emissions in the intertropical discontinuity region of the West African Monsoon, submitted to *Journal of Geophysical Research*, 2009] which examined the dynamics of the monsoon flow along the ITD and associated dust emissions by means of airborne lidar observations and model simulations, respectively. The remainder of the paper is outlined as follows. After the introduction, the data sources including the model and the observations are presented in section 2. The vortex formation, life cycle and thermodynamical characteristics are described in section 3. In section 4, dust emission and transport associated with dry cyclogenesis is discussed. Finally, conclusions are given in section 5.

2. Data Sources

[8] In this study, we use a combination of European Centre for Medium-Range Weather Forecast (ECMWF) analyses, numerical simulations from a mesoscale atmospheric model and spaceborne observations to characterize the environment of the dry cyclones in the ITD, their thermodynamics and dynamics, as well as their impact on dust emissions. These data sets are now described.

2.1. ECMWF Operational Analyses

[9] Synoptic-scale meteorological conditions were established using 6-hourly ECMWF analyses of sea level pressure, horizontal winds at 925 hPa and potential temperature at 925 hPa. In addition, ECMWF analyses were used to compute the temporal evolution of Froude and Rossby numbers in regions upstream of orographic blocking (i.e., Libya) relevant to monitoring of conditions favorable to lee cyclogenesis (see section 3).

2.2. Mesoscale Simulations

[10] MesoNH is a nonhydrostatic mesoscale atmospheric model with an online dust emission and transport module. The capability of MesoNH to simulate dust emission and transport over West Africa has been highlighted in several recent studies [e.g., *Grini et al.*, 2006; *Tulet et al.*, 2008; *Crumeyrolle et al.*, 2008; Bou Karam et al., submitted manuscript, 2009]. MesoNH [*Lafore et al.*, 1997] contains different sets of parameterizations such as cloud microphysics [*Cohard and Pinty*, 2000], turbulence [*Bougeault and Lacarrère*, 1989], convection [*Bechtold et al.*, 2001], lightning processes [*Barthe et al.*, 2005], gaseous chemistry [*Suhre et al.*, 1998], chemical aerosol [*Tulet et al.*, 2005] and dust aerosol [*Grini et al.*, 2006].

[11] MesoNH is coupled to an externalized surface model which handles heat and water vapor fluxes between the low-level atmosphere and four types of surface: vegetation, towns, oceans and lakes [*Masson et al.*, 2003]. Natural land surfaces are described by interactions treated in the Soil Biosphere and Atmosphere model (ISBA) [*Noilhan and Mahfouf*, 1996].

[12] The dust emission scheme is the Dust Entrainment And Deposition (DEAD) model [*Zender et al.*, 2003], implemented as a component of MesoNH [*Grini et al.*, 2006] that calculates dust flux from wind friction speeds. DEAD

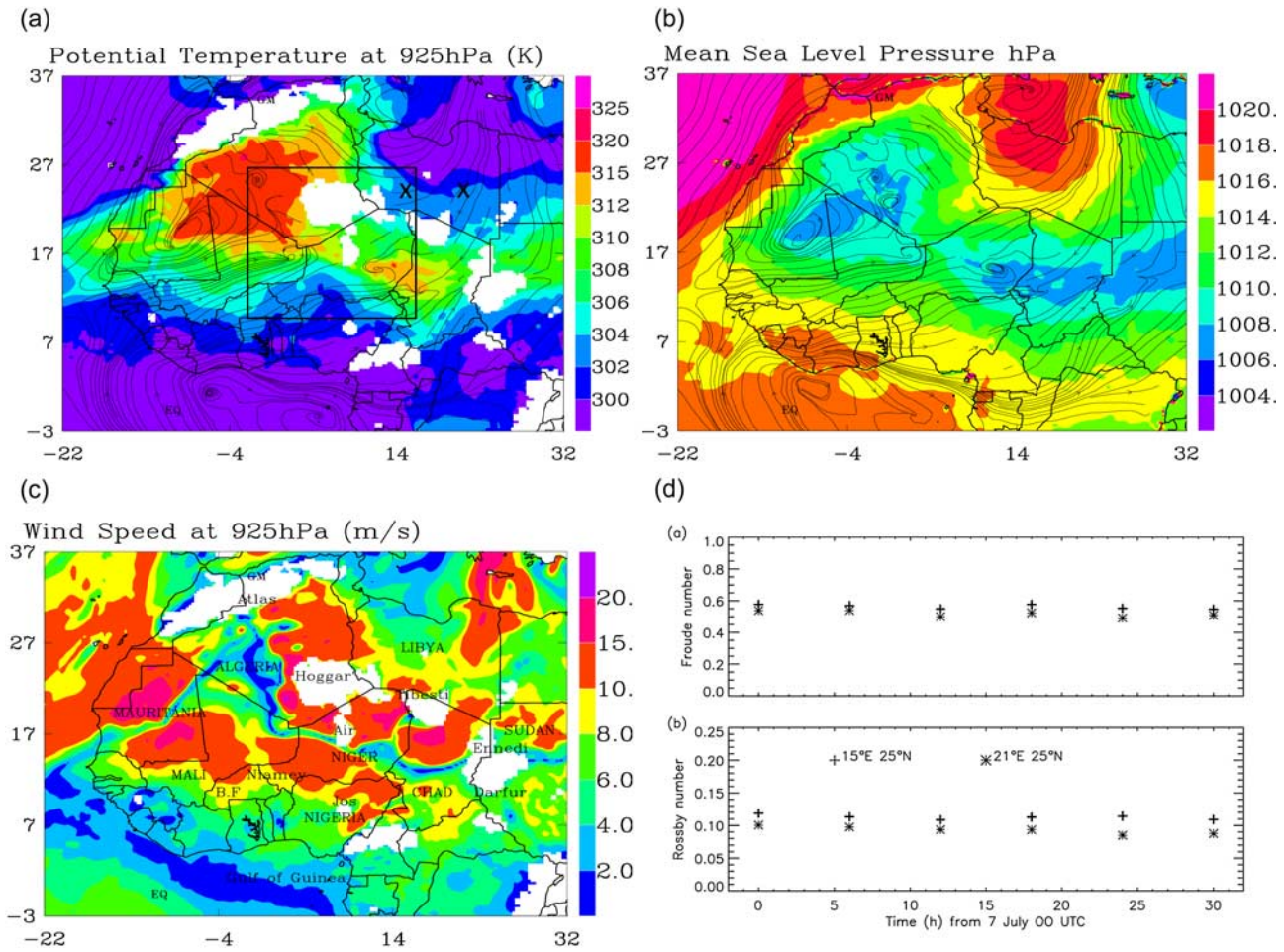

Figure 1. ECMWF analysis on 7 July 2006 at 0600 UTC: (a) potential temperature (colors) and streamlines at 925 hPa, (b) mean sea level pressure (colors) and streamlines at 1 km msl, and (c) wind speed (colors) and streamlines at 925 hPa. The *x* axis represents longitudes and *y* axis represents latitudes. The main orographic features referred to in the text appear in white. The domain of the MesoNH simulation is defined by the black box in Figure 1a. (d) Temporal evolution of the (top) Froude and (bottom) Rossby numbers at 15°E/25°N (pluses) and 21°E/25°N (asterisks) over Libya. See text for details on the computation of Froude and Rossby numbers. The location of the two points used for the calculations of the Froude and the Rossby numbers is marked by black crosses in Figure 1a.

includes entrainment thresholds for saltation, moisture inhibition and saltation feedback. The ORILAM model [*Tulet et al.*, 2005] simulates transport and loss processes by following the evolution of two moments of three lognormal modes defined by *Alfaro and Gomes* [2001]. The ORILAM deposition processes include sedimentation, turbulent mixout, nucleation and washout in cloud [*Mari et al.*, 2000]. Dust advection and diffusion are quantified by the transport processes and methods used in MesoNH which include mixing within the planetary boundary layer, shallow convective transport and advection by winds.

[13] Two 4-day simulations (4–8 July 2006) were designed: one with orography and one without orography, in order to evaluate the role of the mountains on the cyclogenesis within the heat trough. The study area covering Niger, Eastern Mali and southern Algeria forms a domain of 2000 km × 2000 km with a horizontal mesh size of 10 km (see Figure 1a). In the vertical, 72 stretched levels were used. The highest level is at 37 km. The simulations are initialized by the ECMWF analyses.

2.3. Observations

[14] Near infrared vertically integrated water vapor contents, derived from observations from the MOderate Resolution Imaging Spectroradiometer (MODIS, http://modis.gsfc.nasa.gov) instrument aboard the Terra satellite over the area of interest are used for model validation from a thermodynamical point of view. MODIS uses two near-infrared bands centered at 748 and 869 nm. The large difference of integrated water vapor content between the moist monsoon flow to the south of the ITD and the dry harmattan flow to the north of the ITD is used to delineate the position of the ITD.

[15] The horizontal distribution of dust is described using Meteosat Second Generation (MSG) Spinning Enhanced Visible and Infra Red Imager (SEVIRI) images produced from a combination of three infrared channels, namely channel 10

(12 μm), channel 9 (10.8 μm) and channel 7 (8.7 μm). False-color images (available on http://radagast.nerc-essc.ac.uk/SEVIRI_Dust.shtml) are created using an algorithm developed by EUMETSAT which colors red the difference between the 12.0- and 10.8-μm channels, green the difference between the 10.8- and 8.7-μm channels and blue the 10.8-μm channel [e.g., *Schepanski et al.*, 2007]. On these composite images, dust appears pink or magenta.

[16] Finally, information about the vertical distribution of dust over Sahel-Sahara during the event under scrutiny is provided from attenuated backscatter profiles (or reflectivity profiles) at 532 nm retrieved from the spaceborne Cloud-Aerosol LIdar with Orthogonal Polarization (CALIOP) onboard the CALIPSO (Cloud-Aerosol Lidar and Infrared Pathfinder Satellite Observation) [*Winker et al.*, 2003] satellite with vertical and horizontal resolutions of 60 m and 12 km, respectively.

[17] The lidar-derived atmospheric reflectivity at 532 nm is mostly sensitive to aerosols with radii ranging from 0.1 to 5 μm, and hence to dust aerosols [e.g., *Flamant et al.*, 2007]. Furthermore, reflectivity is sensitive to aerosol optical properties and concentration, as well as relative humidity in the case of hygroscopic aerosols. However, over the African continent, close to the sources, desert dust particles are generally considered to be hygrophobic [e.g., *Fan et al.*, 2004]. Therefore, reflectivity associated with desert dust is generally not expected to be sensitive to relative humidity fluctuations, and hence is a good proxy for dust concentration in the atmosphere.

3. Dry Cyclogenesis in the ITD on 7 July 2006

[18] Two main dynamical ingredients were responsible for dry cyclogenesis over western Niger: the orographic blocking and the horizontal shear along the ITD. After describing the synoptic conditions on 7 July 2006, we will detail the contribution of each mechanism to dry cyclogenesis.

3.1. Synoptic Conditions

[19] Using the ECMWF analyses (Figure 1), meteorological conditions over West Africa on 7 July 2006 at 0600 UTC are illustrated. The streamlines and potential temperature field at 925 hPa show evidence of cold air advection from the Mediterranean Sea toward Libya blocked by the Hoggar and the Tibesti mountains, whose tops extend above the 925 hPa surface (Figure 1a). The general circulation over West Africa was driven by the large latitudinal pressure gradient between the continent and the ocean illustrated in the mean sea level pressure field (Figure 1b). At 925 hPa the region south of the zonal band of minimum pressure was under the influence of the southwest monsoon, while to the north, the wind field was under the influence of the Libyan High and was modulated by the topography (Figure 1c). Air masses coming from the north were deflected around the northern flank of the Hoggar toward the Atlas Mountains and in the lee of the constriction between the Tibesti and Hoggar massifs, as well as between the Aïr and Hoggar massifs. Strong southwesterly winds were associated with the monsoon flow over Mali and Niger separated from the strong northeasterly winds by a northwest-southeast oriented line of weak winds corresponding to the ITD located around 17°N to the southwest of the Hoggar and Aïr mountains (Figure 1c), within a low-pressure area which represents the heat trough (Figure 1b). The low-level prevailing northeasterly flow splits upstream of the Hoggar-Tibesti into three branches, with one to the north of the Hoggar, the second one around the southern edge of the Hoggar and the third one to the east of the Tibesti (Figure 1c). These jets provided the background shear vorticity for the development of vortices in the region.

3.2. Windward Flow Characterization

[20] When analyzing the upstream conditions favorable to the development of lee vortices, two parameters controlling the overall flow structure impinging on an obstacle such as a mountain, are generally considered: the Froude number and the Rossby number in the linear theory [*Smith*, 1982, 1989]. The Froude number, which characterize the tendency of the airflow to be lifted or to be driven around the mountains, is defined as

$$\mathrm{Fr} = \mathrm{U}/(\mathrm{N}\,\mathrm{h}), \tag{1}$$

where U is wind speed perpendicular to mountain, h is terrain height, and N is Brunt–Vaisala frequency where $N^2 = (g/\theta)(d\theta/dz)$, with θ the potential temperature. The Rossby number is defined as

$$\mathrm{Ro} = \mathrm{U}/\mathrm{fL}, \tag{2}$$

where f is the Coriolis parameter and L is the characteristic width of the terrain. It measures the relative importance of inertial and Coriolis forces. The Coriolis force becomes small as Ro increases.

[21] The cold air intrusion from the Mediterranean Sea described above was blocked by the Hoggar and the Tibesti ranges. The Froude and Rossby numbers during the study period were calculated from the evolution of the ECMWF analyses in two locations (21°E/25°N and 15°E/25°N) on the windward side located under the cold air masses, using equations (1) and (2) for an average terrain height of 1000 m above mean sea level (msl). The flow on the windward side over the whole period was characterized by a Froude number of about 0.5 and a Rossby number of 0.12 (Figure 1d). These values are within the range of Froude number <1 where upstream blocking and lee vortices form through tilting of baroclinically induced vorticity [*Smolarkiewicz and Rotunno*, 1989; *Rotunno et al.*, 1999]. The Froude and Rossby numbers were also found to be rather insensitive to changes in the average terrain height in the range 1000–2000 m (not shown).

[22] The Rossby number is within the range of intermediate values ($0 < \mathrm{Ro} < 1$) where the Coriolis force becomes significant and the flow curves cyclonically when approaching the mountain, anticyclonically near the ridge, and cyclonically again on the leeside [*Pierrehumbert*, 1984]. In addition, with Fr number values close to 0.5, the impinging flow below the mountain top is blocked by the mountain. Flow splitting upstream produces strong low-level jets (LLJs) both to the northwest and southeast of the Hoggar-Aïr Mountains and forces the air parcels above the mountain tops to sink on the leeside directly from high altitudes (Figure 1c). As the elevated flow sinks on the leeside, high-momentum air from the midtroposphere is entrained and mixed downward to the surface. This surge of high momentum at the surface con-

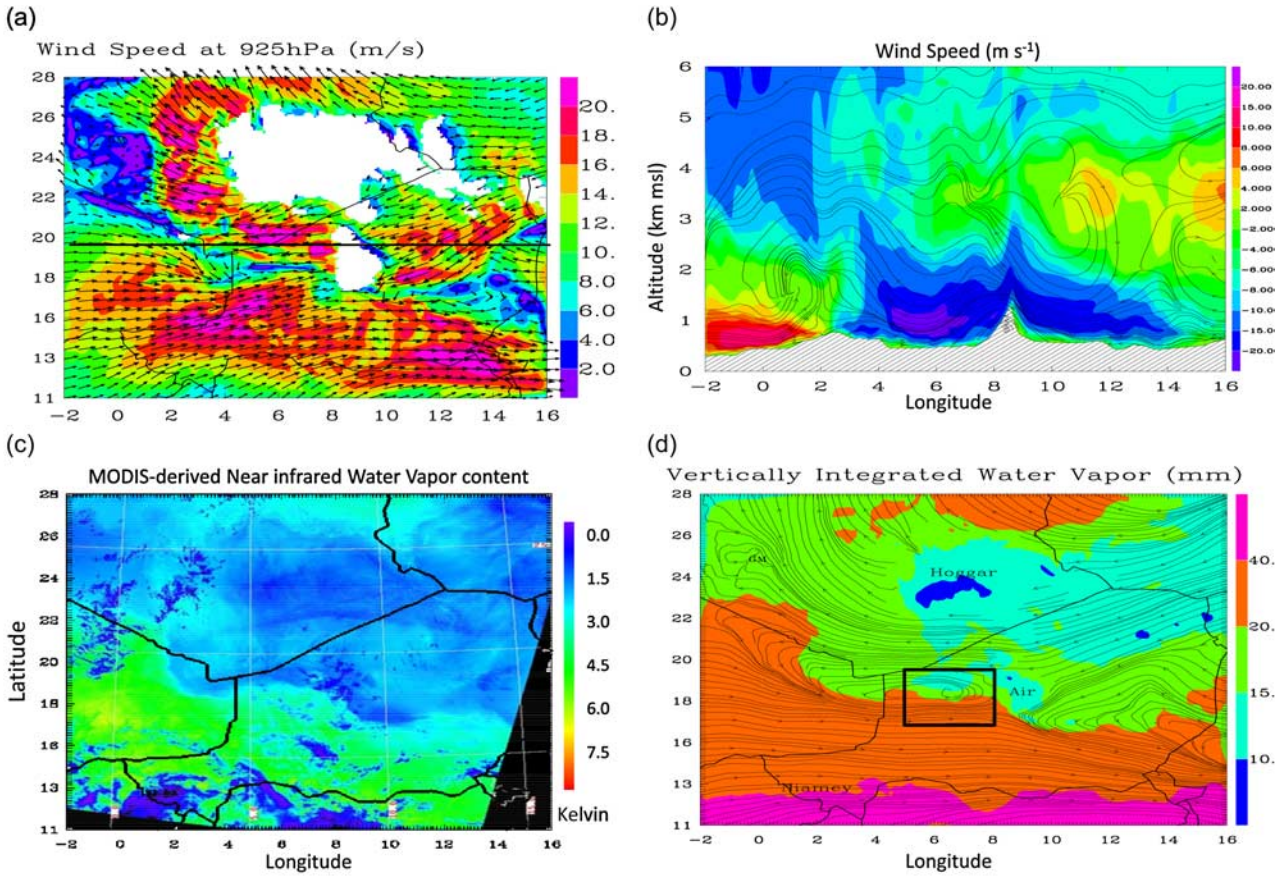

Figure 2. (a) Wind speed at 925 hPa (color) derived from the MesoNH simulation at 0600 UTC on 7 July and wind vectors at the same level superimposed (arrows). (b) Vertical cross section at 20°N (along the black line shown in Figure 2a) of wind speed (color) and streamlines at 0600 UTC on 7 July. (c) MODIS-derived integrated water vapor content field on 7 July at 1020 UTC. (d) Simulated fields of integrated water vapor on 7 July at 1000 UTC (colors) and streamlines at 1 km msl. The black box in Figure 2d represents the subdomain used for the calculation of dew point temperature, zonal wind, and potential vorticity temporal evolution shown in Figure 3.

tributes to an increase in surface velocity as well as frontogenesis around the lee vortex and enhances convergence and cyclonic vorticity within the lee vortex [e.g., *Karyampudi et al.*, 1995].

3.3. Leeside Meteorological Conditions

[23] The orographic blocking of cold air on the windward side as described above led to flow splitting upstream (Figure 2a) producing strong jets at low levels (below 1500 m msl) both to the northwest and southeast of the Hoggar-Aïr Mountains. The topographically constrained LLJs were associated with high wind speeds in excess of 15 m s^{-1} in the same order of those seen in the ECMWF analyses (Figure 1c) with a core of strong winds (20 m s^{-1}) between 800 m and 1200 m msl (Figure 2b).

[24] Southwest of the Hoggar and Aïr mountains, the ITD was located near 17°N latitude as evidenced by the MODIS-derived field of vertically integrated water vapor content on 7 July 2006 at 1020 UTC (Figure 2c). It was observed to undulate over Niger as a result of the influence of the opposing monsoon and harmattan flows as shown in Figure 2d. The details of the horizontal structure of the ITD are captured well by the model (Figure 2d). Also, the contrast in the integrated water vapor content across the ITD on 7 July at 1000 UTC is represented well, with an integrated water vapor content associated with the monsoon of ~30 mm approximately twice that associated with the harmattan of ~15 mm.

[25] In order to characterize the airflow in the ITD region from a thermodynamical point of view, we calculated, in the subdomain 5°E–8°E and 17°N–19°N (see Figures 2b and 2d), the temporal evolution of: (1) the difference of dew-point temperature across the ITD at 10 m above ground level (agl) (Figure 3a), and the difference of the zonal component of wind across the ITD at 10 agl and 1 km msl (Figure 3b). These are obtained from mean values computed on either side of the ITD, within the subdomain, with dew-point temperature and wind values to the north (south) of the ITD characterizing the harmattan (monsoon) flow. The monsoon flow is defined as being characterized by dew point temperatures at 10 m agl in excess of 14°C, while the harmattan is characterized by dew point temperatures less than 14°C [*Buckle*, 1996] (even though Buckle uses dew point temperature at 2 m agl). The average dew point temperature (and zonal wind) value is then derived for the monsoon and the

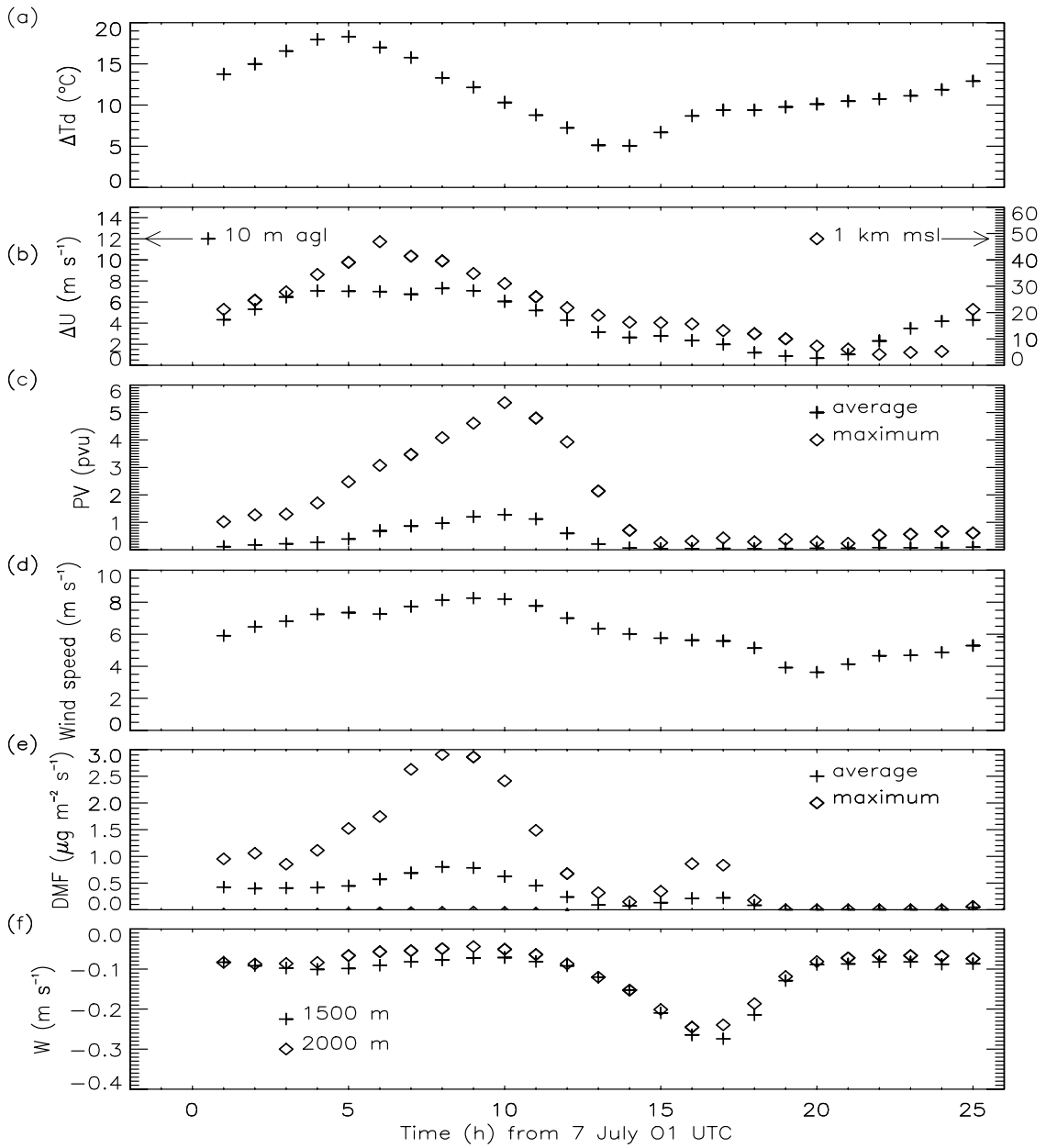

Figure 3. Temporal evolutions between 0100 UTC in 7 July and 0100 UTC on 8 July 2006 of (a) the dew point temperature difference across the ITD, (b) the difference of zonal wind across the ITD at 10 m agl (pluses) and at 1 km msl (diamonds), and (c) the mean (pluses) and maximum (diamonds) of potential vorticity at 1 km msl in the domain shown as a black box in Figure 2b (i.e., covering 5°E–8°E/17°N–19°N). Temporal evolution of (d) the mean of wind speed at 10 m agl and (e) of the mean (pluses) and maximum (diamonds) of dust mass flux in the domain shown as a black box in Figure 7b (i.e., covering 7°E–9°E/19°N–21°N). (f) Temporal evolution of the mean negative vertical velocity at 1500 m msl (pluses) and 2000 m msl (diamonds) in the domain shown as the black box in Figure 4b (i.e., covering 7°E–9°E/19°N–22°N).

harmattan regions in the subdomain, and the difference is determined, for each hourly MesoNH output field. Large values of the differences of dew point temperature and/or zonal wind component are expected when the ITD is well defined and horizontal shear across it is substantial.

[26] A maximum contrast in dew-point temperature (19°C) is observed at 0500 UTC on 7 July, while differences remain in excess of 10°C until 1100 UTC (Figure 3a). The airflow in the ITD was characterized by a strong horizontal shear at 1 km msl, with a difference of wind speed across the ITD in excess of 30 m s^{-1} between 0200 and 0900 UTC (Figure 3b) in connection with the surges of the nocturnal monsoon flow [e.g., *Parker et al.*, 2005; *Lothon et al.*, 2008]. The maximum of wind speed difference across the ITD at 1 km msl is close to 50 m s^{-1} at 0600 UTC (Figure 3b).

[27] The strong horizontal shear between the harmattan and the monsoon seen in the simulation around 0700 UTC (40 m s^{-1}) is similar to that observed in the airborne Doppler lidar observations on 7 July as discussed by *Bou Karam et al.* [2008]. In these observations, at low levels (below 2000 m msl), northeasterly harmattan characterized by a wind speed (direction) of about 20 m s^{-1} (100°) and southwesterly monsoon characterized by a wind speed (direction) of about 18 m s^{-1} (250°) were evidenced across the ITD around 0700 UTC which was located near 18.5°N along the flight track. These wind conditions were realistically reproduced along the aircraft flight track in the simulation Bou Karam et al., submitted manuscript, 2009).

[28] Hence, because strong horizontal shear in the low levels favors the formation of vortices [e.g., *Asai and Miura*, 1981; *Nagata*, 1993] and the production of cyclonic vorticity necessary for the maintenance of the vortices in the low levels [e.g., *Krishnamurti et al.*, 1981], more favorable conditions for dry cyclogenesis in the ITD are expected during night and in the morning hours.

3.4. Characteristics of the 7 July 2006 Vortex

[29] Three vortices were seen in the simulation during the 24-h period under investigation. The first vortex developed in the morning of 7 July 2006 and was centered over northwestern Niger, while the two other vortices developed in the evening of 7 July over northeastern Mali and eastern Niger. In this study, we focus on the first of these, mostly because of availability of observations.

[30] In the morning of 7 July (i.e., 0600 UTC), before the appearance of the cyclone in the wind field at 1 km msl, the pronounced horizontal shear at this level (i.e., evidenced by the large wind speed difference across the ITD on the order of 50 m s^{-1}, Figure 3b) exerts a counterclockwise torque on the air parcels in the vicinity of the ITD and initiates cyclogenesis. The localized rotation initiated in altitude, where the maximum counterclockwise torque by the ambient flow is present, was followed by the transfer of angular momentum to the surface [e.g., *Lemon and Doswell*, 1979]. Evidence of this transfer can be seen in the slight increase in the wind difference across the ITD at 0900 UTC (Figure 3b). The decrease of wind speed difference across the ITD at 1 km msl (Figure 3b) in the interval 0600–1000 UTC accompanies the increase of potential vorticity at 1 km msl (Figure 3c) in the same time interval.

[31] The cyclone was visible in the ITD region after 0700 UTC over western Niger to the west of the Aïr Mountains (centered on 6°E/18.5°N; see Figure 4a) as evidenced by a closed circulation in the wind field below 1500 m msl. The cyclone was no longer seen in the simulation after 1400 UTC. It was quite stationary between 0700 and 1300 UTC. Cyclogenesis (i.e., development and strengthening of the cyclonic circulation) was observed between 0700 and 1000 UTC as evident from Figure 3c which shows that the potential vorticity in the region of the cyclone reached a maximum at 1000 UTC (in excess of 5 PVU). Averaged (maximum) potential vorticity values of 0.9 and 1.1 PVU (3–5.5 PVU) were associated with the vortex center during its intensification stage (Figures 4a and 3c). Cyclolysis (i.e., weakening of the cyclonic circulation) was observed between 1100 and 1300 UTC, as evident from the decrease in potential vorticity in the area of the cyclone. The diameter of the cyclone (as delineated from the streamlines field at 1 km msl) was found to be largest at 1100 UTC and on the order of 400 km (Figure 4b).

[32] A vertical cross section through the cyclone shows strong ascendance (0.20 m s^{-1}) near 6.5°N (Figure 5a) associated with the cyclone center. These strong ascendant motions resulted in the formation of shallow clouds at the top of the planetary boundary layer near the vortex center as one can see in the MODIS near-infrared image (Figure 2c). In this region, the planetary boundary layer was observed to be deepest and vertical mixing strongest (Figure 5b).

[33] Model results for the simulation without orography (Figure 4c) also show the formation of a cyclone in the region of the ITD, even though the cyclone appeared to be centered at 9°E/17°N, i.e., farther southeast than the cyclone in the simulation with orography (Figure 4b). This indicates that the orography, upon wind intensification through generation of LLJs, tends to move the place of vortex initiation to the favorable location to the lee of the Hoggar-Aïr Mountains, thereby influencing the location of dry cyclogenesis initiation in the ITD region.

[34] The vortex in the simulation without orography formed later (0900 UTC), had a shorter lifespan (3 h) and was weaker than in the simulation with the orography. Between 0900 and 1300 UTC, the position of the cyclonic circulation in the simulation without orography was stationary. The cyclogenesis period was from 0900 to 1100 UTC as evident from Figure 4d. Potential vorticity was observed to be largest at the vortex center at 1100 UTC, both for the maximum and average values (∼4 PVU and 1.05 PVU, respectively; Figure 4d), i.e., smaller values than those in the simulation with orography (∼5.5 PVU and 1.1 PVU, respectively, Figure 3c). At 1100 UTC, the cyclone was characterized by a horizontal diameter of roughly 200 km, i.e., half the cyclone diameter in the simulation with orography.

[35] The comparison of the characteristics of the vortex in the simulations with and without orography suggests that the orography plays a secondary but important role in the formation of the cyclone. Orography and related flow splitting tend to create LLJs in the lee of the Hoggar-Aïr mountains which, in turn, create conditions favorable to the onset of a better defined (as shown from streamlines) and more intense (as shown from potential vorticity) vortex in the ITD region. Moreover, orography blocking appears to favor the occurrence of a longer-lived cyclone, as also discussed by *Horvath et al.* [2006]. In both simulations, the cyclones were seen to be quite stationary. More importantly, these results suggest that dry cyclones may form over the Sahel along the entire ITD and not only over the region situated in the lee of mountains.

[36] The cyclone seen in the simulation with orography is also present in the ECMWF analyses. At 1200 UTC, the cyclone under scrutiny is apparent in the ECMWF analyses wind field at 1 km msl (Figure 6a) and is located in approximately the same position as in the MesoNH simulation (Figure 6b), even though slightly displaced to the east, closer to the Aïr Mountains. The second cyclone seen in the MesoNH simulation over southeastern Niger is also present in the ECMWF analysis at 1200 UTC. Overall, the potential temperature and wind fields at 1 km msl from Meso-NH

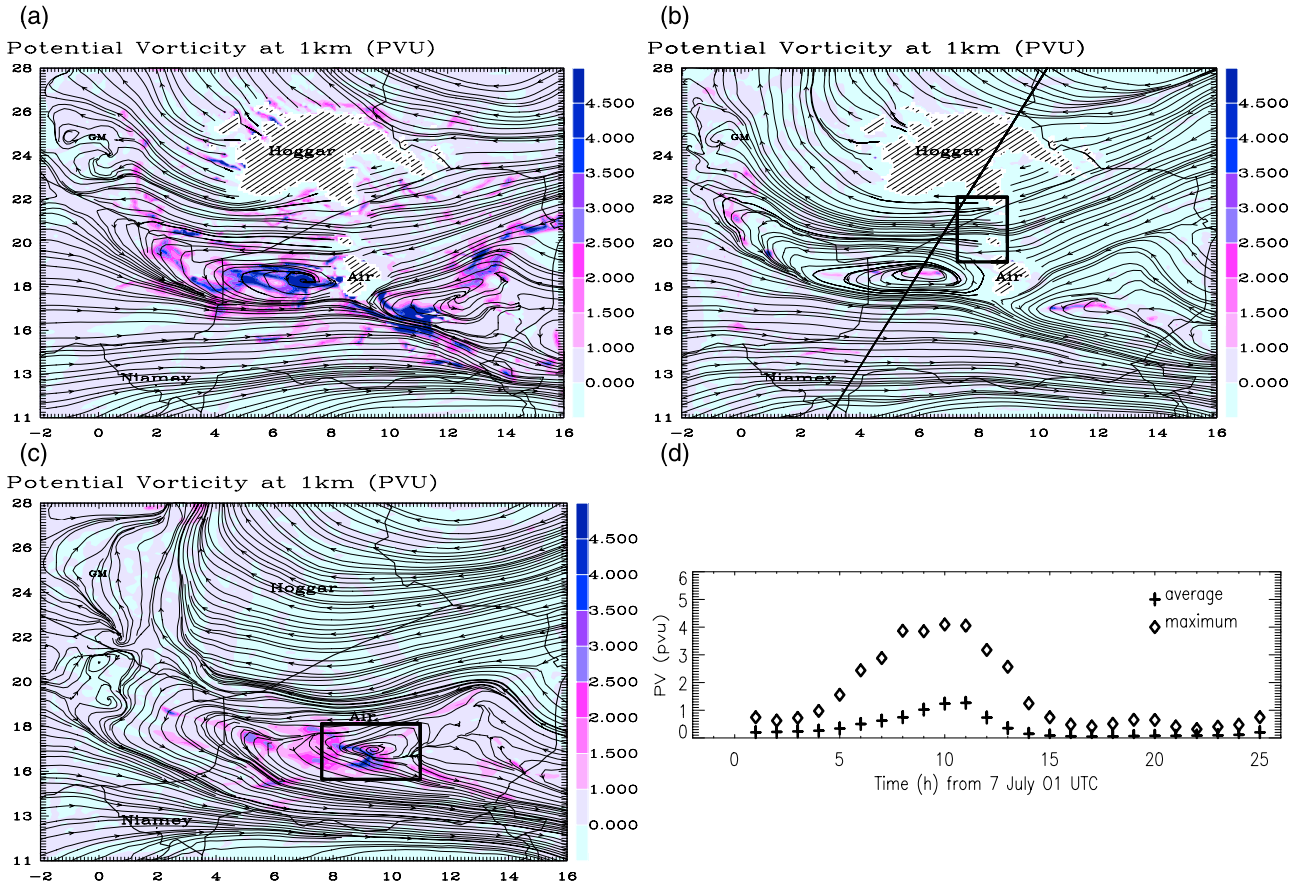

Figure 4. Potential vorticity in PVU (colors) and streamlines at 1 km at 0700UTC (a) and 1100 UTC (b) on 7 July for the simulation with orography. (c) Same as Figure 4b, but for the simulation without orography. (d) Temporal evolutions between 0100 UTC in 7 July and 0100 UTC on 8 July 2006 of average (pluses) and maximum (diamonds) potential vorticity for the simulation without topography, in the domain shown as a black box in Figure 4c i.e., covering 8°E–11°E/16°N–18°N. The black box in Figure 4b represents the subdomain used for the calculation of the temporal evolution of the average of vertical velocity shown in Figure 3e.

and ECMWF are consistent (Figure 6), even though there are some small differences due to higher horizontal resolution of the MesoNH simulation.

[37] The fact that the ITD cyclones can be seen in the ECMWF analyses is important to report, as they could be used to establish climatology of these features during the monsoon season, using for example the ECMWF ERA-40 reanalysis data. Even though establishing such climatology is beyond the scope of this paper, we have attempted to assess the representativeness of the cyclonic event analyzed in this study. Inspecting the ECMWF analyses wind fields at 925 hPa over 2 months (June and July) during the monsoon season of 2006, we were able to identify over 110 cyclonic events occurring along the entire ITD over the continent. This suggests that dry cyclogenesis in the ITD region occurs often and may have a significant impact on the atmospheric dynamics in West Africa.

4. Dust Emission and Transport Associated With Dry Cyclogenesis

[38] The decrease of wind speed difference across the ITD at 1 km msl (Figure 3b) during the cyclogenesis period is connected to a diminution of the wind speed on either side of the ITD at this altitude (not shown). It was accompanied by an increase of the wind at the surface around the vortex. The simulation provides evidence that during the cyclogenesis phase (0700–1000 UTC), characterized by the transfer of angular momentum from 1 to 1.5 km msl to the surface, the surface winds along the northeastern edge of the vortex increased and reached a maximum of 8 m s^{-1} on average (Figure 3d), while locally reaching maximum values of 11 m s^{-1} (suitable for dust lofting, not shown). At 1100 UTC, at the beginning of the cyclolysis phase, high surface winds of 7 m s^{-1} on average (Figure 3d) and a local maximum in excess of 9 m s^{-1} (Figure 7a) are still seen along the northeastern branch of the vortex even though not as strong as during cyclogenesis.

[39] The strong surface winds associated with the vortex dynamics are responsible for the lofting of dust in a region well known to be a dust source area, and characterized by the existence of a huge system of ephemeral rivers and streams that drain the Hoggar and Aïr massifs, which define a complex array of dust sources consisting of fluvial deposits. A recent study by *Schepanski et al.* [2007] has shown that this area is a prominent dust source in the summer season, being

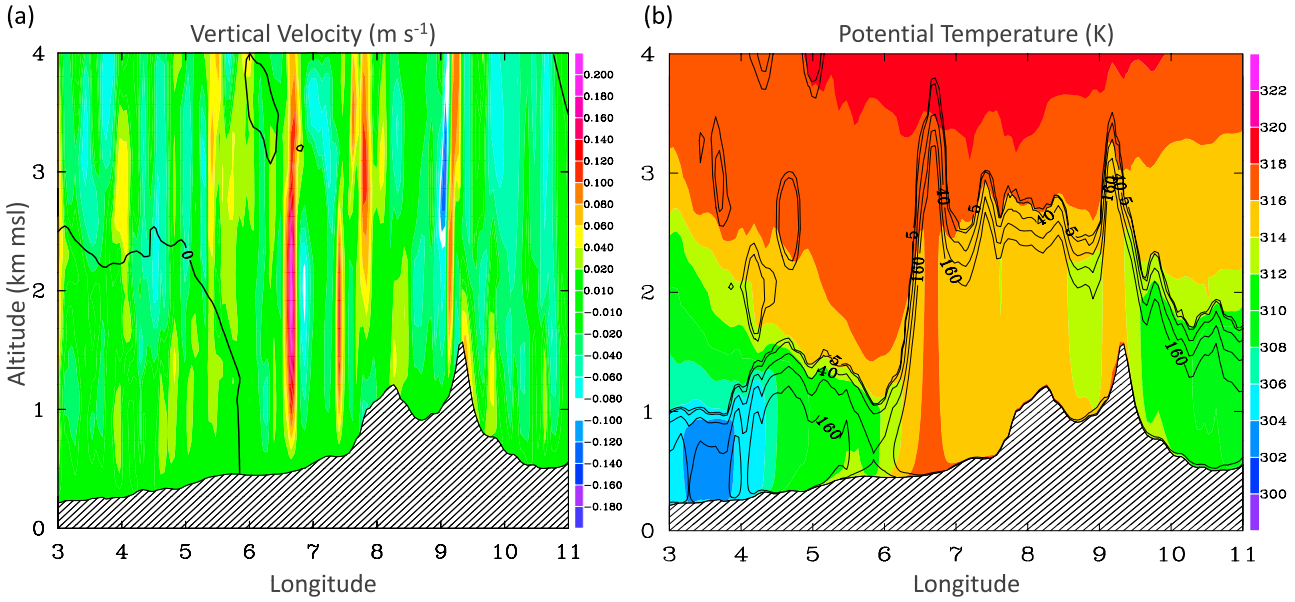

Figure 5. Vertical cross section along the black line shown on Figure 4b on 7 July at 1100 UTC of (a) vertical velocity and (b) potential temperature (color) and turbulent kinetic energy (contours). The thick black line in Figure 5a corresponds to the zero isotach in the winds perpendicular to the cross section delineated the ITD.

located in the vicinity of mountain foothills where fluvial sediment provides fine material for deflation. These enhanced dust mass fluxes are simulated in the region of large near surface winds (Figure 7b). The related dust mass flux was seen to peak around 0.7–0.8 μg m^{-2} s^{-1}, on average, between 0600 and 1100 UTC in the area of maximum dust emission (Figure 3e), even though local maximum values of dust mass flux in excess of 2 μg m^{-2} s^{-1} were simulated (Figure 3e). The peak in dust flux mass was observed at 0800 UTC (Figure 3e), i.e., during the intensification stage of the cyclone characterized by local maximum values of potential vorticity in excess of 4 PVU (Figure 3c).

[40] It is worth noting that the dust emissions were initiated by high surface winds generated by the enhancement of the cyclonic vorticity associated with the intensification of the vortex rather than by an increase of the mountain downslope winds. At least the largest dust mass flux values were calculated (Figure 3e) during the few hours following the cyclone initiation. On the other hand and during the same period, a negative correlation between the dust flux (Figure 3e)

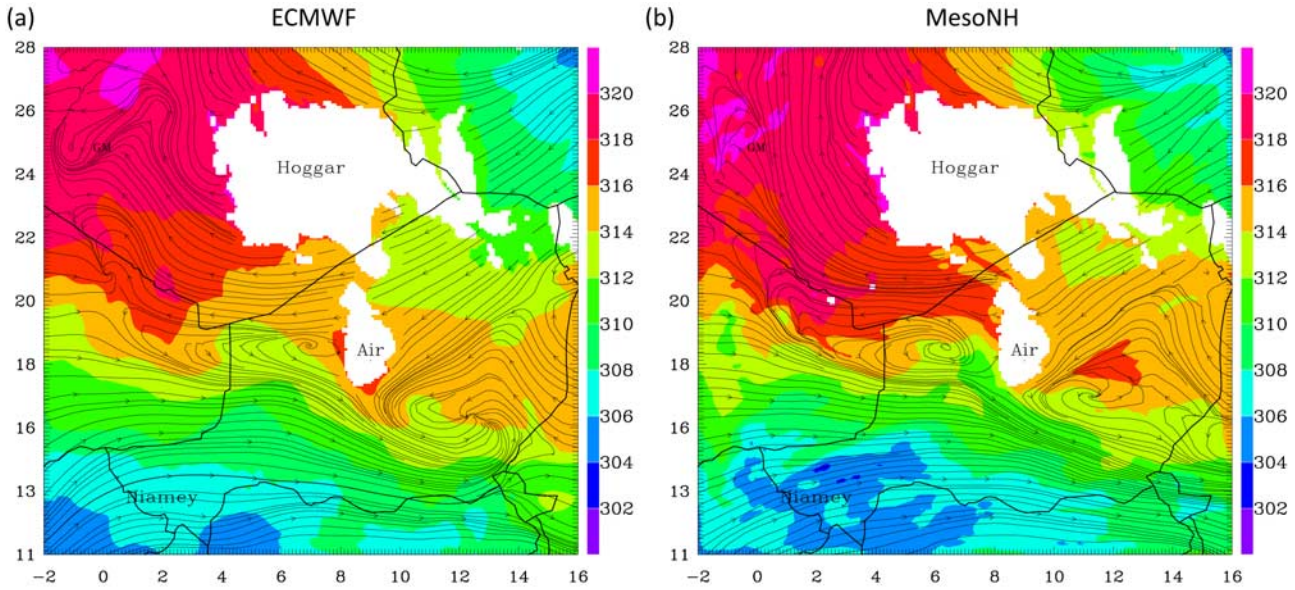

Figure 6. Potential temperature field at 1 km msl (colors) on 7 July 2006 at 1200 UTC, (a) resulting from the projection of the ECMWF analyses on the study domain and (b) simulated by MesoNH. Streamlines at 1 km msl are superimposed in black.

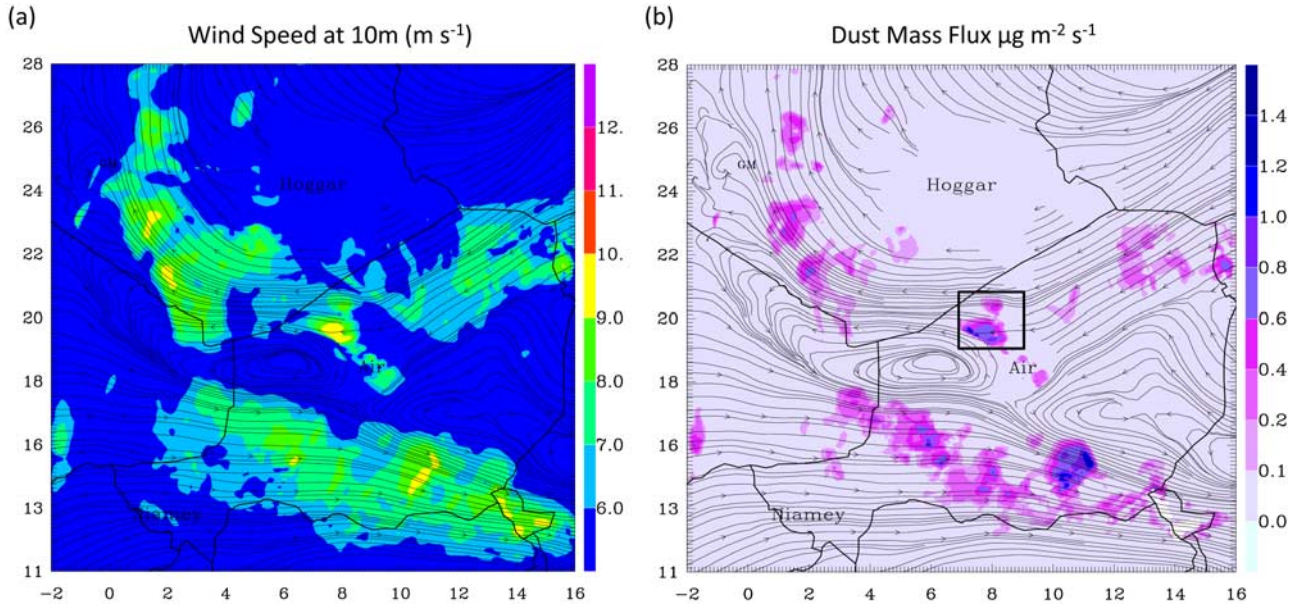

Figure 7. (a) Simulated wind speeds at 10 m above ground level (agl, color) with overlain streamlines at 1 km (above msl) on 7 July at 0011 UTC and (b) dust mass flux derived from the MesoNH simulation at 1100 UTC on 7 July. The black box in Figure 7b represents the subdomain used for the calculation of the temporal evolution of the dust mass flux shown in Figure 3 at 1100 UTC.

and the negative vertical velocity in the lee of the Hoggar is seen (Figure 3f), suggesting that the enhanced near surface winds were not caused by enhanced downslope winds.

[41] It should be noted that to the south, over southern Niger the large dust mass fluxes (e.g., Figure 7b) simulated in the region of strong monsoonal winds along the southern edge of the ITD are related to the mechanism described by *Bou Karam et al.* [2008] in which highly turbulent winds behind the leading edge of the monsoon flow generate dust lofting. This paper is not concerned with that particular phenomenon.

[42] The dust was drawn upward by the turbulent flow of air from ground level into the vortex core (Figure 8a). A vertical cross section of dust concentration through the vortex shows a coherent vertical plume located near 6.5°E/19°N (Figure 8b) and reaching roughly 3 km msl with higher concentration (2000 μg m^{-3}) between the ground and 1800 m msl. The dust plume was most developed in the

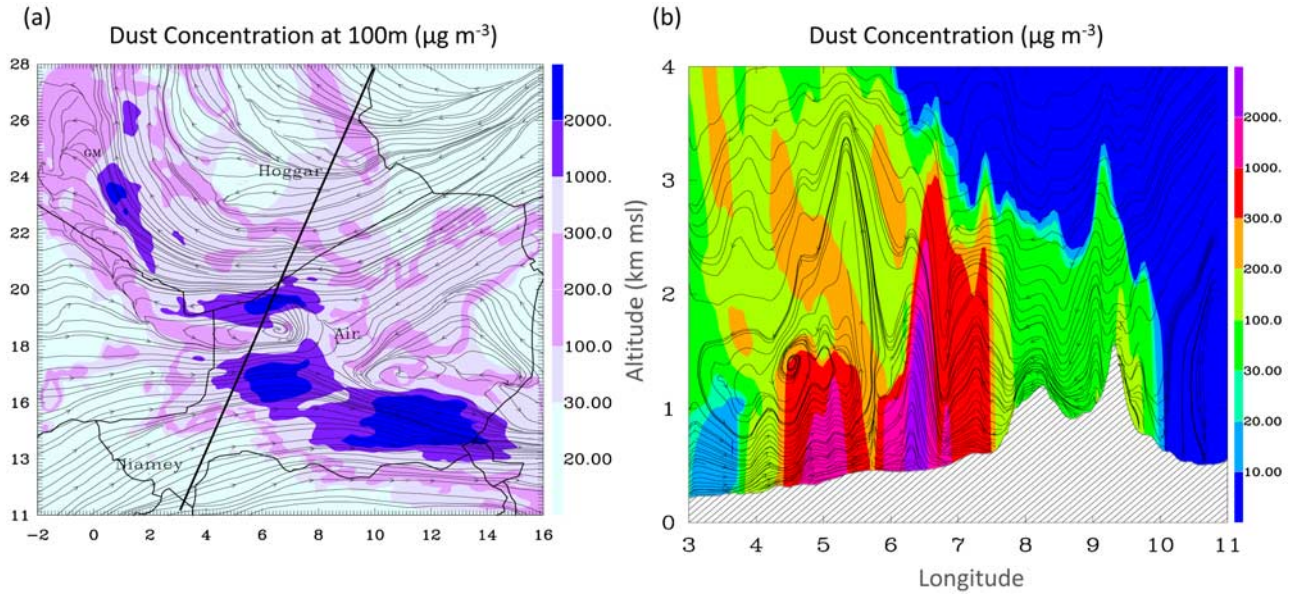

Figure 8. (a) Dust concentrations (color) derived from MesoNH simulation and streamlines at 100 m agl at 1100 UTC on 7 July. (b) Vertical cross section through the cyclone along the black line shown in Figure 8a of dust concentrations (color) and streamlines at 1100 UTC on 7 July.

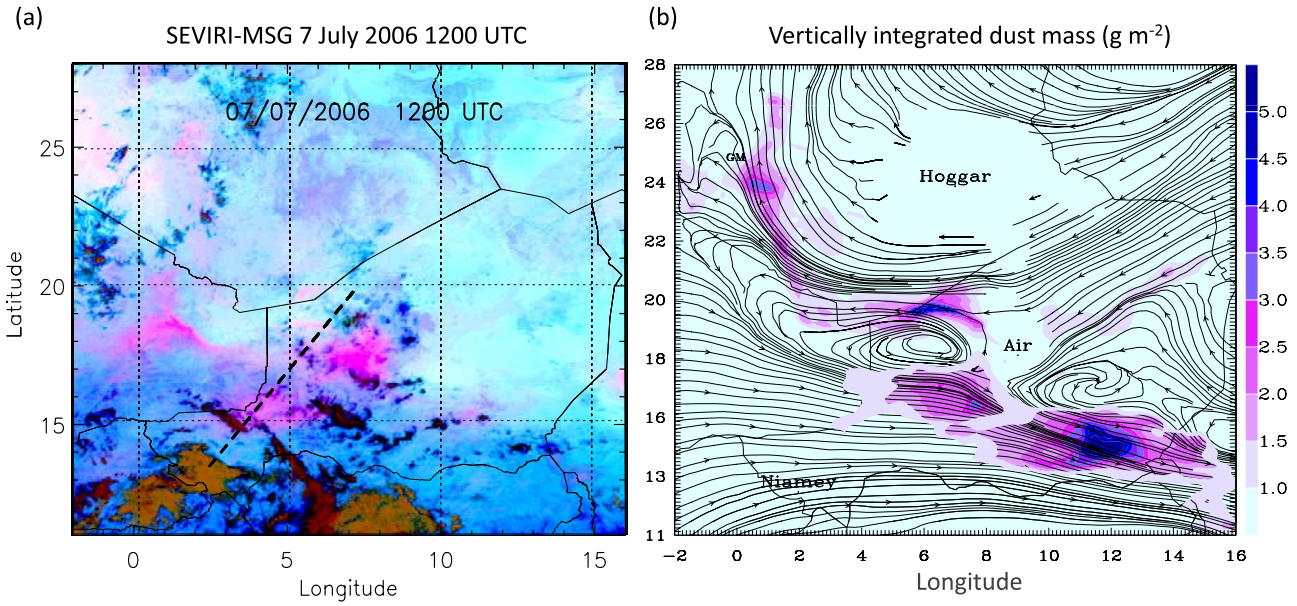

Figure 9. (a) SEVIRI-MSG false-color image on 7 July 2006 at 1200 UTC in which dusts appear in pink or magenta, water vapor is dark blue, thick high-level clouds are red-brown, thin high-level clouds are almost black, and surface features are pale blue or purple. (b) Simulated field of vertically integrated dust mass on 7 July at 1200 UTC (colors) and streamlines at 1 km msl.

region of strong ascendance associated with the cyclone dynamics as discussed earlier. This suggests that the described mechanism offers a means for rapid injection of the mobilized dust to high altitudes, especially near the vortex center, where strong ascending motions are consistently present (i.e., Figure 5a).

[43] The SEVIRI-MSG false color image on 7 July 2006 at 1200 UTC (in which dusts appear in pink or magenta, Figure 9a), evidences the presence of a (faint) dust plume, along the northern edge of the cyclone (i.e., close to 6°E, 19°N). A better defined dust plume is observed along the ITD (roughly along 18°N), as well as farther south, around 15°E/5°N. The latter is likely caused by the strong winds and the turbulence associated with the leading edge of the cold pool of a convective system observed near Niamey (as in work by *Flamant et al.* [2007]), and is not reproduced in the simulation (owing to the lack of a moist convective system). The lifting along the edge of the ITD is well simulated in the model. There has been some discussion of the applicability of these images (as the dust effect on brightness temperature differences depends on its altitude [e.g., *Pierangelo et al.*, 2004]), suggesting that they may favor only dust which is elevated so that its radiating temperature differs significantly from the ground. In this case, the consistency between the observations and the simulation along the ITD confirms that the dust at the leading edge of the monsoon flow is lifted sufficiently to be apparent in the satellite imagery. On the other hand, the dust lifted as the result of the action of the cyclone is likely not lifted to sufficient height at this time to be apparent in the SEVIRI false color composition. This is confirmed by the fact that the dust lifted by the cyclone was more evident in the SEVIRI observations later on the day (i.e., from 1300 UTC on). The dust load associated with the action of the cyclone is estimated to be as large as 5 g m^{-2} (Figure 9b).

[44] Inspection of the simulated dust fields suggests that the dust mobilized during the cyclogenesis event was mixed to altitudes of about 4–5 km msl during the rest of the day and remained in the atmosphere after the cyclone had disappeared. It then experienced westward advection during the afternoon hours and was observed in the SEVIRI-MSG image over Eastern Mali during the night on 8 July (Figures 10a and 10b). The plume was advected as a coherent vertical structure, until sunset, and experienced tilting afterward, i.e., from 2000 UTC on. The tilting of the plume as seen in the CALIPSO spaceborne lidar observations (Figure 10c) was imposed by the nighttime advance of the monsoon flow which advected the plume to the north in the lower levels, while the top of the plume was advected southwestward by the northeasterly harmattan winds to the south. This deformation of the initially vertical plume led to a southward-tilted plume over eastern Mali by midnight as suggested also by the model dust concentration field along CALIPSO track (Figure 10c).

[45] Even though this result is based on a single case, it suggests that the dust mobilized and mixed through the depth of the Sahelian planetary boundary layer can experience long-range transport and may impact the radiative budget over a larger area and for a longer time period than the cyclone size and lifespan, respectively.

5. Conclusions

[46] Mesoscale numerical simulations as well as satellite observations were investigated to highlight the formation of dry cyclones in the ITD region of West Africa and their impacts on dust emission and transport over the Sahel.

[47] Model results show the development of the vortex to be associated with (1) strong horizontal shear and low-level convergence existing along the ITD and (2) enhanced

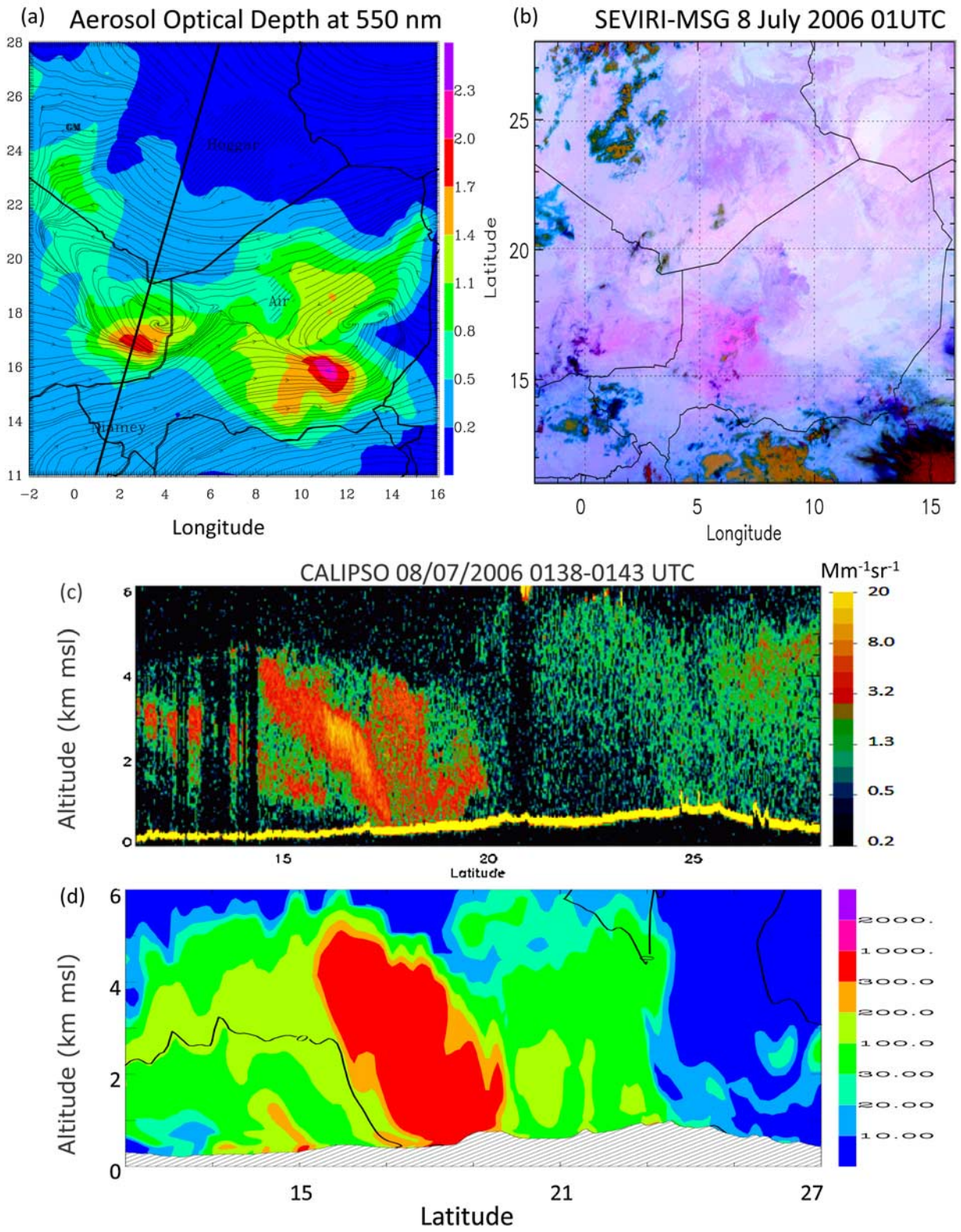

Figure 10. (a) Simulated field of Aerosol Optical Depth at 550 nm on 8 July at 0100 UTC (color) and streamlines at 1 km msl. (b) SEVIRI-MSG false-color image on 8 July at 01 UTC. (c) Lidar backscatter coefficient profiles at 532 nm along the CALIPSO transect (black line in Figure 10a) over West Africa on 8 July 2006 at 0130 UTC. (d) Simulated dust concentration at 0100 UTC along CALIPSO track. The thick black line represents the isotach zero wind and delineates the ITD position.

northeasterly winds associated with Hoggar-Aïr Mountains orographic blocking of air masses advected from the Mediterranean Sea.

[48] Dry cyclogenesis was initiated in altitude where the ambient flow was characterized by a strong horizontal shear across the ITD (i.e., a wind speed difference of nearly 50 m s^{-1} at 1 km msl) due to the existence of strong opposing winds (a northeasterly one forced by orography and the monsoon southwesterly winds). The initiation in altitude was then followed by a transfer of angular momentum to the surface.

[49] Strong surface velocity associated with the vortex dynamics and enhanced by the strong opposing winds was at the origin of dust mobilization. The uplifted dust was made available for long-range transport after being mixed up to 5 km in altitude and advected westward. Dry cyclogenesis in the ITD region over the Sahel seems to offer an efficient mechanism for dust uplifting and injection into higher altitudes, thereby making the airborne dust available for long-range transport.

[50] More importantly, the results suggest that dry cyclogenesis may occur over the Sahara-Sahel along the entire ITD and not only over the region situated in the lee of mountains. These results were confirmed by the inspection of the ECMWF analyses of wind field at 925 hPa which revealed the formation of over 110 dry cyclones along the entire ITD during June and July 2006.

[51] In addition, dry cyclogenesis over the Sahel-Sahara offers an efficient dynamical forcing for the transfer of elevated high wind speeds to the surface which, unlike the breakdown of the nocturnal LLJs by the turbulent mixing, does not request surface heating. This suggests that the downward mixing of LLJs momentum to the surface by the dynamical forcing linked to cyclogenesis and related dust emissions could occur during night and in the morning hours and not necessarily after sunrise, and hence contribute significantly to the total dust activity over West Africa.

[52] This study details a mechanism for dust mobilization over Sahara-Sahel during the monsoon season when the annual peak of dust emissions is observed but remains underestimated by regional model (e.g., K. Schepanski et al., Meteorological processes forcing Saharan dust emission inferred from MSG-SEVIRI observations of subdaily dust source activation, submitted to *Journal of Geophysical Research*, 2009). The described mechanism supports the hypothesis given by *Engelstaedter and Washington* [2007] in which dust emissions over West Africa correlates well with gustiness and dry convection, but not so much with the mean surface winds. Our results provide also a possible explanation for the climatological results by *Engelstaedter and Washington* [2007]. The fact that the peak in the annual dust cycle over West Africa is found in June/July is also consistent with the fact that the ITD is generally located over the West African dust hot spots during this period.

[53] Further investigation is needed to substantiate these findings, in particular the seasonal and annual frequency of dry cyclogenesis over West Africa and its correlation with the annual dust activity need to be addressed in future studies in order to evaluate the contribution of the highlighted mechanism to the total dust production over West Africa.

[54] Observational documentation of dry cyclogenesis in the West African ITD is highly needed to better understand their associated mechanisms involved on dust emission and transport as well as the interactions of vortices with other dynamical features over West Africa, i.e., tropical cyclones.

[55] In the analysis of the 7 July 2006 case study reported here and by *Bou Karam et al.* [2008] we have identified two specific dust generating processes, the nocturnal monsoon flow south of the ITD and dry cyclogenesis within the ITD. In doing so we are building a clearer picture of the complex processes involved in dust emission and transport during the important summer dust season in West Africa.

[56] **Acknowledgments.** On the basis of a French initiative, AMMA was built by an international scientific group and is currently funded by a large number of agencies, especially from France, UK, U.S. and Africa. It has been the beneficiary of a major financial contribution from the European Community's Sixth Framework Research Programme. Detailed information on scientific coordination and funding is available on the AMMA International web site http://www.ammainternational.org. Discussions with P. Knippertz are most appreciated. J.-P. Chaboureau is acknowledged for providing the ECMWF analyses data, and B. Francis is acknowledged for designing Figure 2c. Computer resources were allocated by the "Institut de Développement et des Ressources en Informatique Scientifique" (IDRIS). E.R.W.'s contribution to this study was supported by NASA contract NNX07AT036 and by NSF ATM 0734806.

References

Alfaro, S. C., and L. Gomes (2001), Modeling mineral aerosol production by wind erosion: Emission intensities and aerosol size distributions in source areas, *J. Geophys. Res.*, *106*(D16), 18,075–18,084.

Asai, T., and Y. Miura (1981), An analytical study of meso-scale vortex-like disturbances observed around Wakasa Bay area, *J. Meteorol. Soc. Jpn.*, *59*, 832–843.

Barthe, C., G. Molini, and J. Pinty (2005), Description and first results of an explicit electrical scheme in a 3d cloud resolving model, *Atmos. Res.*, *76*(1-4), 95–113.

Bechtold, P., E. Bazile, F. Guichard, P. Mascart, and E. Richard (2001), A mass-flux convection scheme for regional and global models, *Q. J. R. Meteorol. Soc.*, *127*, 869–886, doi:10.1002/qj.49712757309.

Bougeault, P., and P. Lacarrère (1989), Parameterization of orography-induced turbulence in a mesobeta-scale model, *Mon. Weather Rev.*, *117*(8), 1872–1890, doi:10.1175/1520-0493(1989)117<1872:POOITI>2.0.CO;2.

Bou Karam, D., C. Flamant, P. Knippertz, O. Reitebuch, M. Chong, J. Pelon, and A. Dabas (2008), Dust emissions over the Sahel associated with the West African Monsoon inter-tropical discontinuity region: A representative case study, *Q. J. R. Meteorol. Soc.*, *134*, 621–634, doi:10.1002/qj.244.

Briegel, L. M., and W. M. Frank (1997), Large-scale influences on tropical cyclogenesis in the western North Pacific, *Mon. Weather Rev.*, *125*, 1397–1413.

Buckle, C. (1996), *Weather and Climate in Africa*, Addison-Wesley, Harlow, U. K.

Cohard, J., and J. Pinty (2000), A comprehensive two moments warm microphysical bulk scheme: 2d experiments with a non hydrostatic model, *Q. J. R. Meteorol. Soc.*, *126*, 1843–1859, doi:10.1256/smsqj.56614.

Crumeyrolle, S., L. Gomes, P. Tulet, A. Matsuki, A. Schwarzenboeck, and K. Crahan (2008), Increase of the aerosol hygroscopicity by aqueous mixing in a mesoscale convective system: A case study from the AMMA campaign, *Atmos. Chem. Phys. Discuss.*, *8*, 10,057–10,103.

Engelstaedter, S., and R. Washington (2007), Atmospheric controls on the annual cycle of North African dust, *J. Geophys. Res.*, *112*, D03103, doi:10.1029/2006JD007195.

Fan, S. M., L. W. Horowitz, H. Levy II, and W. J. Moxim (2004), Impact of air pollution on wet deposition of mineral dust aerosols, *Geophys. Res. Lett.*, *31*, L02104, doi:10.1029/2003GL018501.

Flamant, C., J. P. Chaboureau, D. P. Parker, C. M. Taylor, J. P. Cammas, O. Bock, F. Timouk, and J. Pelon (2007), Airborne observations of the impact of a convective system on the planetary boundary layer thermodynamics and aerosol distribution in the inter-tropical discontinuity region of the West African Monsoon, *Q. J. R. Meteorol. Soc.*, *133*, 1175–1189, doi:10.1002/qj.97.

Grini, A., P. Tulet, and L. Gomes (2006), Dusty weather forecasts using the Meso-NH mesoscale atmospheric model, *J. Geophys. Res.*, *111*, D19205, doi:10.1029/2005JD007007.

Horvath, K., L. Fita, R. Romero, B. Ivancan-Picek, and I. Stiperski (2006), Cyclogenesis in the lee of the Atlas Mountains: A factor separation numerical study, *Adv. Geosci.*, *7*, 327–331.

Karyampudi, V. M., and H. F. Pierce (2002), Synoptic-scale influence of the Saharan air layer on tropical cyclogenesis over the eastern Atlantic, *Mon. Weather Rev.*, *130*(12), 3100–3128, doi:10.1175/1520-0493(2002)130<3100:SSIOTS>2.0.CO;2.

Karyampudi, V. M., M. L. Kaplan, S. E. Koch, and R. J. Zamora (1995), The influence of the Rocky Mountains in the 13–14 April 1986 severe weather outbreaks. Part I: Mesoscale lee cyclogenesis and its relationship to severe weather and dust storms, *Mon. Weather Rev.*, *123*(5), 1394–1422, doi:10.1175/1520-0493(1995)123<1394:TIOTRM>2.0.CO;2.

Krishnamurti, T., P. Ardanuy, Y. Ramanathan, and R. Pasch (1981), On the onset vortex of the summer monsoon, *Mon. Weather Rev.*, *109*, 344–363.

Lafore, J. P., et al. (1997), The Meso-NH Atmospheric Simulation System. Part I: Adiabatic formulation and control simulations, *Ann. Geophys.*, *16*, 90–109, doi:10.1007/s00585-997-0090-6.

Lander, M., and G. J. Holland (1993), On the interaction of tropical-cyclone-scale vortices. I: Observations, *Q. J. R. Meteorol. Soc.*, *119*, 1347–1361.

Lemon, L. R., and C. A. Doswell (1979), Severe thunderstorm evolution and mesocyclone structure as related to tornadogenesis, *Mon. Weather Rev.*, *107*, 1184–1197, doi:10.1175/1520-0493(1979)107<1184:STEAMS>2.0.CO;2.

Liu, M., D. L. Westphal, S. Wang, A. Shimizu, N. Sugimoto, J. Zhou, and Y. Chen (2003), A high-resolution numerical study of the Asian dust storms of April 2001, *J. Geophys. Res.*, *108*(D23), 8653, doi:10.1029/2002JD003178.

Lothon, M., F. Saïd, F. Lohou, and B. Campistron (2008), Observation of the diurnal cycle of the low troposphere of West Africa and impact on the transport of water vapour, *Mon. Weather Rev.*, *136*(9), 3477–3500, doi:10.1175/2008MWR2427.1.

Mari, C., D. Jacob, and P. Bechtold (2000), Transport and scavenging of soluble gases in a deep convective cloud, *J. Geophys. Res.*, *105*(D17), 22,255–22,263.

Masson, V., J.-L. Champeaux, F. Chauvin, C. Meriguet, and R. Lacaze (2003), A global database of land surface parameters at 1km resolution in meteorological and climate models, *J. Clim.*, *16*, 1261–1282.

Nagata, M. (1993), Meso-β-scale vortices developing along the Japan-sea polar-airmass convergence zone (JPCZ) cloud band: Numerical simulation, *J. Meteorol. Soc. Jpn.*, *71*, 43–57.

Noilhan, J., and J. F. Mahfouf (1996), The ISBA land surface parameterization scheme, *Global Planet. Change*, *13*, 145–159, doi:10.1016/0921-8181(95)00043-7.

Parker, D. J., R. R. Burton, A. Diongue-Niang, R. J. Ellis, M. Felton, C. M. Taylor, C. D. Thorncroft, P. Bessemoulin, and A. M. Tompkins (2005), The diurnal cycle of the west African monsoon circulation, *Q. J. R. Meteorol. Soc.*, *131*, 2839–2860, doi:10.1256/qj.04.52.

Pierangelo, C., A. Chédin, S. Heilliette, N. Jacquinet-Husson, and R. Armante (2004), Dust altitude and infrared optical depth from AIRS, *Atmos. Chem. Phys.*, *4*, 1813–1822.

Pierrehumbert, R. T. (1984), Linear results on the barrier effects of Mesoscale Mountains, *J. Atmos. Sci.*, *41*, 1356–1367, doi:10.1175/1520-0469(1984)041<1356:LROTBE>2.0.CO;2.

Prospero, J. M., P. Ginoux, O. Torres, S. E. Nicholson, and T. E. Gill (2002), Environmental characterization of global sources of atmospheric soil dust identified with the Nimbus 7 Total Ozone Mapping Spectrometer (TOMS) absorbing aerosol product, *Rev. Geophys.*, *40*(1), 1002, doi:10.1029/2000RG000095.

Qian, W., L. Quan, and S. Shi (2002), Variations of the dust storms in China and its climatic control, *J. Clim.*, *15*, 1216–1229, doi:10.1175/1520-0442(2002)015<1216:VOTDSI>2.0.CO;2.

Redelsperger, J.-L., C. D. Thorncroft, A. Diedhiou, T. Lebel, D. J. Parker, and J. Polcher (2006), African Monsoon Multidisciplinary Analysis: An international research project and field campaign, *Bull. Am. Meteorol. Soc.*, *87*, 1739–1746, doi:10.1175/BAMS-87-12-1739.

Rotunno, R., V. Grubisic, and P. K. Smolarkiewicz (1999), Vorticity and potential vorticity in mountain wakes, *J. Atmos. Sci.*, *56*, 2796–2810, doi:10.1175/1520-0469(1999)056<2796:VAPVIM>2.0.CO;2.

Sadler, J. C. (1975), The upper tropospheric circulation over the global tropics, *Atlas UHMET 75–05*, 35 pp., Dep. of Meteorol. Univ. of Hawaii, Honolulu.

Schepanski, K., I. Tegen, B. Laurent, B. Heinold, and A. Macke (2007), A new Saharan dust source activation frequency map derived from MSG-SEVIRI IR channels, *Geophys. Res. Lett.*, *34*, L18803, doi:10.1029/2007GL030168.

Smith, R. B. (1982), Synoptic observations and theory of orographically disturbed wind and pressure, *J. Atmos. Sci.*, *39*, 60–70, doi:10.1175/1520-0469(1982)039<0060:SOATOO>2.0.CO;2.

Smith, R. B. (1989), Hydrostatic flow over mountains, *Adv. Geophys.*, *31*, 1–41.

Smolarkiewicz, P. K., and R. Rotunno (1989), Low Froude number flow past three-dimensional obstacles. Part I: Baroclinically generated lee vortices, *J. Atmos. Sci.*, *46*, 1154–1164, doi:10.1175/1520-0469(1989)046<1154:LFNFPT>2.0.CO;2.

Suhre, K., et al. (1998), Physico-chemical modeling of the first aerosol characterization experiment (ACE 1) Lagrangian b: 1. A moving column approach, *J. Geophys. Res.*, *103*(D13), 16,433–16,455, doi:10.1029/98JD00821.

Toyoda, E., H. Niino, K. Tsuboki, and R. Kimura (1999), Midtropospheric anticyclonic vortex street associated with a cloud band near a cold front, *J. Atmos. Sci.*, *56*, 2637–2656.

Tulet, P., V. Crassier, F. Cousin, K. Suhre, and R. Rosset (2005), ORILAM, a three-moment lognormal aerosol scheme for mesoscale atmospheric model: Online coupling into the Meso-NH-C model and validation on the Escompte campaign, *J. Geophys. Res.*, *110*, D18201, doi:10.1029/2004JD005716.

Tulet, P., M. Mallet, V. Pont, J. Pelon, and A. Boone (2008), The 7–13 March 2006 dust storm over West Africa: Generation, transport, and vertical stratification, *J. Geophys. Res.*, *113*, D00C08, doi:10.1029/2008JD009871.

Winker, D. M., J. Pelon, and M. P. McCormick (2003), The CALIPSO mission: Spaceborne lidar for observation of aerosols and clouds, *Proc. SPIE Int. Soc. Opt. Eng.*, *4893*, 1–11.

Zender, C., H. Bian, and D. Newman (2003), The mineral dust entrainment and deposition model DEAD: Description and 1990s dust climatology, *J. Geophys. Res.*, *108*(D14), 4416, doi:10.1029/2002JD002775.

D. Bou Karam, C. Flamant, and J. Pelon, LATMOS, IPSL, Université Pierre et Marie Curie, CNRS, tour 45/46, 3° etage, boite 308, 4, Place Jussieu, F-75005 Paris, France. (diana@aero.jussieu.fr)

M. C. Todd, Department of Geography, University College London, Pearson Building, Gower Street, London WC1E 6BT, UK. (m.todd@geog.ucl.ac.uk)

P. Tulet, GAME, CNRM, Météo-France, Toulouse, France.

E. Williams, Lincoln Laboratory, Massachusetts Institute of Technology, S1-641, 244 Wood Street, Lexington, MA 02420-9108, USA.